

A Hybrid Simulation Method for Radiative Transfer Equations

M. JUNK¹, A. UNTERREITER² and F. ZINGSHEIM³

¹ *Universität Kaiserslautern, D-67663 Kaiserslautern, Germany*
email: junk@mathematik.uni-kl.de

² *TU Berlin, Institut für Mathematik, MA 6-3, 10623 Berlin, Germany*
email: unterreiter@math.tu-berlin.de

³ *LMS Deutschland GmbH, Luxemburger Strasse 7, D-67657 Kaiserslautern, Germany*
email: Frank.Zingsheim@lms-ge.de

(Received)

We consider heat transfer processes where radiation in a large number of frequency bands plays a dominant role. In the simulation of such processes, the radiative transfer equation has to be solved repeatedly. To obtain an efficient and accurate solution method, we propose a new hybrid algorithm which combines fast solvers for the radiative transfer equation in the low and high absorption regime, respectively. A key role is played by an exact, residual based error formula. The algorithm is applied to a cooling problem of high quality optical glass.

Key words. heat equation; stationary radiative transfer equation; hybrid method; normed residuum; projection method; frequency bands; high absorption limit; cooling processes.

AMS(MOS) subject classification. 35F15, 35Q60, 80A20, 80M25.

1 Introduction

We are concerned with heat transfer processes where the heat flux is strongly influenced by radiation. The corresponding mathematical model consists of the heat equation coupled with the stationary radiative transfer equation (RTE). The coupling is obtained via the sources: a temperature field leads to a field of radiation sources and the radiative energy transport effects the temperature evolution by causing a non-local heat flux. The numerical simulation of such a process requires a time discretization of the heat equation and in each time step, the RTE has to be solved with new sources to obtain the radiative heat flux.

Consequently, the choice of the RTE-solver influences the quality and the overall speed of the simulation decisively. Classical methods like ray tracing or P_N approximations are too slow to obtain reasonable simulation times. Faster methods, like the ROSSELAND approximation, typically perform well only in specific frequency bands.

Since we are dealing with a large number of frequency bands ranging from very small to very high frequencies, such a single asymptotic approximation is inadequate. We propose

a new hybrid method which combines two fast algorithms designed for high and low absorption rates, respectively. The decision which solver is to be used in a frequency band is based on an error formula for approximate solutions of the RTE: a weighted integral over the residuum of any approximate solution of the RTE yields an expression for the distance to the exact solution in a natural norm. For a detailed investigation of this residual based error formula, we refer to [4].

The resulting algorithm is implemented for an application arising in glass industry in connection with the production of high quality, optical glass: a too fast cooling of the glass may lead to internal stresses which degrade the quality or even cause breakage. On the other hand, slow cooling is time and energy consuming. Hence the cooling process should be as short as possible but as careful as necessary.

For the design of optimal cooling processes, numerical simulations are very helpful [1, 8] but since long cooling periods have to be simulated, the speed of the RTE solver is a very important aspect. With our algorithm, we obtain a speed which is comparable to the one of the ROSSELAND approximation (which is widely used for the simulation of cooling processes). However, the quality of the results is much better with our algorithm and compares to the precision obtained with a (50 times slower) ray tracing method.

The paper is organized as follows. In section 2 we formulate the model equations. The widely used ray tracing, the ROSSELAND and the P_N approximation are briefly described in sections 3.1, 3.2, 3.3. The new hybrid method is developed in section 3.4. Simulation results for cooling processes are contained in section 3.5. Comparisons of the results with respective results from standard methods are included.

2 The Model

We consider a non scattering semi transparent medium, e.g. high quality glass, confined to a bounded domain $G \subseteq \mathbb{R}^3$ with smooth or piecewise smooth boundary (for example, a cylinder or polygon).

We assume that the temperature $T = T(t, \mathbf{x}) > 0$ at time $t > 0$ and position $\mathbf{x} \in G$ in the medium satisfies

$$\eta \frac{\partial T}{\partial t} = \kappa \Delta T - \operatorname{div} \mathbf{F}, \quad (2.1)$$

subject to initial conditions

$$T(0, \mathbf{x}) = T_0(\mathbf{x}) \quad (2.2)$$

and to homogeneous Neumann boundary conditions

$$\nabla T \cdot \mathbf{n} = 0, \quad \text{on } \partial G, \quad (2.3)$$

where $\eta > 0$ is the product of the medium's mass density and the specific heat capacity (for constant volume), $\kappa > 0$ is the thermal conductivity, \mathbf{n} is the outward unit normal vector along the boundary ∂G of G . The Neumann boundary conditions of (2.3) refer to an insulating boundary. Extensions to more general heat transfer models can easily be performed but are not employed for the sake of simplicity.

In (2.1) the energy flux due to radiation, $\mathbf{F} = \mathbf{F}(t, \mathbf{x})$, plays a key role. The vector-

valued function \mathbf{F} is given by

$$\mathbf{F}(t, \mathbf{x}) = \int_{(0, \infty) \times S^2} \boldsymbol{\xi} \cdot I(t, \boldsymbol{\xi}, \mathbf{x}, \nu) d(\nu, \omega(\boldsymbol{\xi})), \quad (2.4)$$

where $I(t, \boldsymbol{\xi}, \mathbf{x}, \nu)$ is the medium's radiative intensity of frequency $\nu \in (0, \infty)$ in direction $\boldsymbol{\xi} \in S^2$, S^2 the unit sphere in \mathbb{R}^3 , at (t, \mathbf{x}) , and $d(\nu, \omega(\boldsymbol{\xi}))$ denotes integration with respect to the standard product measure on $(0, \infty) \times S^2$.

We assume that radiation transport is much faster than the time evolution of the temperature. As a consequence, the radiative intensities $I = I(t, \boldsymbol{\xi}, \mathbf{x}, \nu)$ shall satisfy for each $t > 0$ the *stationary* radiative transfer equation [5, 6, 7]

$$\frac{1}{\sigma(\nu)} \boldsymbol{\xi} \cdot \nabla I + I = n_m^2 \beta(T, \nu), \quad \text{for } (\boldsymbol{\xi}, \mathbf{x}) \in S^2 \times G, \nu \in (0, \infty) \quad (2.5)$$

where $\sigma(\cdot)$ is the (positive) absorption coefficient function (depending on the frequency ν), $n_m > 0$ is the refraction index of the medium and

$$\beta : (0, \infty) \times (0, \infty) \rightarrow (0, \infty), \quad \beta(T, \nu) = \frac{4\pi\hbar\nu^3}{c^2 \left(\exp\left(\frac{2\pi\hbar\nu}{k_B T}\right) - 1 \right)},$$

is Planck's radiation function where \hbar is Planck's constant, c is the speed of light in vacuum and k_B is Boltzmann's constant. We note that both T and ν enter in (2.5) as parameters while the directional space derivative $\boldsymbol{\xi} \cdot \nabla$ couples $\boldsymbol{\xi}$ and \mathbf{x} dependence.

Equation (2.5) is supplemented with modified FRESNEL boundary conditions for the intensity $I = I(t, \boldsymbol{\xi}, \boldsymbol{\zeta}, \nu)$ which apply on a subset $S^- := \{(\boldsymbol{\xi}, \boldsymbol{\zeta}) \in S^2 \times \partial G : \boldsymbol{\xi} \cdot \mathbf{n}(\boldsymbol{\zeta}) < 0\}$ of the boundary $S^2 \times \partial G$

$$I = \hat{\rho} I'' + (1 - \hat{\rho}) n_m^2 \beta(T_F, \nu), \quad \text{for } (\boldsymbol{\xi}, \boldsymbol{\zeta}) \in S^- \quad (2.6)$$

where the reflection coefficient function $\hat{\rho} : [0, 1] \rightarrow [0, 1]$ is determined by a FRESNEL-type law and is evaluated at $|\boldsymbol{\xi} \cdot \mathbf{n}(\boldsymbol{\zeta})|$, T_F is an outer reference temperature chosen to approximate the outer background radiation (for the sake of simplicity we assume constant T_F) and I'' denotes the intensity $I(t, \boldsymbol{\xi}'', \boldsymbol{\zeta}, \nu)$ in the reflected direction

$$\boldsymbol{\xi}'' = \boldsymbol{\xi}''(\boldsymbol{\xi}, \mathbf{n}(\boldsymbol{\zeta})) = \boldsymbol{\xi} - 2(\boldsymbol{\xi} \cdot \mathbf{n}(\boldsymbol{\zeta})) \mathbf{n}(\boldsymbol{\zeta}).$$

The treatment of the frequency dependence is simplified considerably if the discrete measurements of the absorption coefficient function $\sigma(\nu)$ are extended to a piecewise constant function. We assume that there are frequencies $0 = \nu_0 < \nu_1 < \dots < \nu_{M-1} < \nu_M = \infty$ such that $\sigma(\nu) = \sigma_k \in (0, \infty)$ in the frequency band $\nu \in [\nu_{k-1}, \nu_k)$, $k = 1, \dots, M$. Introducing frequency integrated intensities $k = 1, \dots, M$,

$$I_k : (0, \infty) \times G \times S^2 \rightarrow [0, \infty), \quad I_k(t, \boldsymbol{\xi}, \mathbf{x}) = \int_{\nu_{k-1}}^{\nu_k} I(t, \boldsymbol{\xi}, \mathbf{x}, \nu) d\nu, \quad (2.7)$$

$$\beta_k : (0, \infty) \rightarrow (0, \infty), \quad \beta_k(T) = \int_{\nu_{k-1}}^{\nu_k} n_m^2 \beta(T, \nu) d\nu, \quad (2.8)$$

as well as the first $\boldsymbol{\xi}$ moment of I_k

$$\mathbf{F}_k : (0, \infty) \times G \rightarrow \mathbb{R}^3, \quad \mathbf{F}_k(t, \mathbf{x}) = \int_{S^2} \boldsymbol{\xi} \cdot I_k(t, \boldsymbol{\xi}, \mathbf{x}) d\omega(\boldsymbol{\xi}), \quad (2.9)$$

we can re-write the model equation (2.1)

$$\eta \frac{\partial T}{\partial t} = \kappa \Delta T - \sum_{k=1}^M \operatorname{div} \mathbf{F}_k, \quad \text{on } (0, \infty) \times G, \quad (2.10)$$

subject to the conditions (2.2) and (2.3). The integrated intensities I_k , $k = 1, \dots, M$, arising in the definition (2.9) of \mathbf{F}_k satisfy for each $t > 0$,

$$\frac{1}{\sigma_k} \boldsymbol{\xi} \cdot \nabla I_k + I_k = \beta_k(T), \quad \text{on } S^2 \times G, \quad (2.11)$$

$$I_k - \hat{\rho} I_k'' = (1 - \hat{\rho}) \beta_k(T_F), \quad \text{for } (\boldsymbol{\xi}, \boldsymbol{\zeta}) \in S^- \quad (2.12)$$

where, again, $\hat{\rho} = \hat{\rho}(|\boldsymbol{\xi} \cdot \mathbf{n}(\boldsymbol{\zeta})|)$ and $I_k''(t, \boldsymbol{\xi}, \boldsymbol{\xi}) = I_k(t, \boldsymbol{\xi}'', \boldsymbol{\zeta})$.

3 Numerical methods and simulations

For the numerical approximations of (2.11), (2.12), a variety of methods has been proposed (see [5], [6], and [9]). They can be subdivided into three main classes:

- Methods where $\boldsymbol{\xi}$ is reduced to a discrete set of directions, such as the ray tracing method or the discrete ordinate method S_N .
- Methods based on asymptotic analysis, for example the ROSSELAND approximation.
- Methods where the $\boldsymbol{\xi}$ -dependence is prescribed in form of special functions, such as the spherical harmonic expansion P_N (Galerkin approach).

In connection with a discretization of (2.10), equations (2.11) and (2.12) have to be solved in each time step. If P_N or S_N approximations are used, large linear systems have to be solved repeatedly. Similarly, the ray tracing method is much too expensive to be used in each step. The ROSSELAND approximation, on the other hand, is very fast but rather inaccurate in frequency bands with low absorption and close to the boundaries of the domain.

Our aim is to construct a new method which is more accurate than the ROSSELAND approach and considerably faster than the P_N or S_N approximation. Before doing this, we briefly describe the methods which we use for comparison.

3.1 The ray tracing method

Applying the method of characteristics to the radiative transfer equation (2.5), we obtain the ray tracing method [5] which is also called discrete transfer model [3]. For a given point $\mathbf{x} \in G$ and some $\boldsymbol{\xi} \in S^2$, we have (with frequency and time dependence suppressed for simplicity)

$$I(\boldsymbol{\xi}, \mathbf{x}) = I(\boldsymbol{\xi}, \mathbf{x} - s\boldsymbol{\xi})e^{-\sigma s} + \sigma n_m^2 \int_0^s \beta(T(\mathbf{x} - \tau\boldsymbol{\xi}))e^{-\sigma\tau} d\tau \quad (3.1)$$

as long as the ray $s \mapsto \mathbf{x} - s\boldsymbol{\xi}$ is inside \bar{G} . If $\boldsymbol{\zeta} = \mathbf{x} - \bar{s}\boldsymbol{\xi} \in \partial G$, the boundary condition (2.6) has to be observed. Since $\boldsymbol{\xi} \cdot \mathbf{n}(\boldsymbol{\zeta}) < 0$, we have

$$I(\boldsymbol{\xi}, \boldsymbol{\zeta}) = \rho I(\boldsymbol{\xi}'', \boldsymbol{\zeta}) + (1 - \rho)n_m^2 \beta(T_F).$$

where $\hat{\rho}$ is evaluated at $|\boldsymbol{\xi} \cdot \mathbf{n}(\boldsymbol{\zeta})|$. To calculate $I(\boldsymbol{\xi}'', \boldsymbol{\zeta})$, we continue with (3.1), where we observe $-\boldsymbol{\xi}'' \cdot \mathbf{n}(\boldsymbol{\zeta}) < 0$. Since the intensity decreases along the ray with a damping factor $e^{-\sigma s}$ as well as by a factor $\hat{\rho}$ in each reflection, the process can practically be stopped after a certain number m of reflections (the number decreases with increasing σ) giving rise to an approximation $I^m(\boldsymbol{\xi}, \mathbf{x})$.

Our main objective in solving RTE is the calculation of the radiative heat flux (2.4). Hence, we need to find the first $\boldsymbol{\xi}$ moment of the intensity. In the context of ray tracing methods, we use quadrature rules

$$\int_{S^2} \boldsymbol{\xi} I(\boldsymbol{\xi}, \mathbf{x}) d\omega(\boldsymbol{\xi}) \approx \sum_{i=1}^N \omega_i^N \boldsymbol{\xi}_i^N I^m(\boldsymbol{\xi}_i^N, \mathbf{x}).$$

For a detailed discussion of suitable weights ω_i^N and directions $\boldsymbol{\xi}_i^N$, we refer to [9].

3.2 The Rosseland approximation

In the case when σ is very large (the optically thick limit), we see from (3.1) that the intensity at some interior point $\mathbf{x} \in G$ is essentially determined through near-by sources. Carrying out a regular expansion in $1/\sigma \rightarrow 0$, the so called ROSSELAND approximation is recovered (see for example [5, 7]), which we use here up to order one:

$$\begin{aligned} I^{(0)}(\boldsymbol{\xi}, \mathbf{x}) &= n_m^2 \beta(T(\mathbf{x})), & \mathbf{x} \in G \\ I^{(0)}(\boldsymbol{\xi}, \boldsymbol{\zeta}) &= n_m^2 \hat{\rho} \beta(T(\boldsymbol{\zeta})) + (1 - \hat{\rho}) n_m^2 \beta(T_F), & (\boldsymbol{\xi}, \boldsymbol{\zeta}) \in S^- \end{aligned}$$

(with $\hat{\rho}$ evaluated at $|\boldsymbol{\xi} \cdot \mathbf{n}(\boldsymbol{\zeta})|$) and

$$\begin{aligned} I^{(1)}(\boldsymbol{\xi}, \mathbf{x}) &= -n_m^2 \boldsymbol{\xi} \cdot \nabla \beta(T(\mathbf{x})), & \mathbf{x} \in G \\ I^{(1)}(\boldsymbol{\xi}, \boldsymbol{\zeta}) &= -n_m^2 \hat{\rho} \boldsymbol{\xi}'' \cdot \nabla \beta(T(\boldsymbol{\zeta})), & (\boldsymbol{\xi}, \boldsymbol{\zeta}) \in S^- \end{aligned}$$

We remark that the intensity is usually discontinuous on the boundary S^- .

3.3 A modified P_N approximation

In the classical P_N approximation, the $\boldsymbol{\xi}$ -dependence of the intensity is expanded in spherical harmonic functions $Y_{kl}(\boldsymbol{\xi})$ of degree $k \in \mathbb{N}_0$, $l = -k, \dots, k$ up to degree N . The resulting expression for I is plugged into the RTE and relations for the space dependent coefficients in the expansion are obtained by multiplying the equation with Y_{kl} and subsequent integration over S^2 . In this process, \mathbb{L}^2 -orthogonality relations of the spherical harmonic functions and recurrence relations are used.

The equations for the different coefficient functions are coupled via the term $\boldsymbol{\xi} \cdot \nabla I = \text{div}(\boldsymbol{\xi} I)$. The resulting differential equations for the coefficients have to be solved in G . Boundary conditions are constructed in analogy. The relation satisfied by the intensity on the subset S^- of the boundary $S^2 \times \partial G$ turns into conditions for *all* coefficients on the *whole* boundary ∂G . In general, these are too many constraints for the problem to be well posed and one has to select a suitable subset of boundary conditions which introduces some arbitrariness.

This problem can be avoided by passing to a weak formulation of the RTE which

contains the boundary conditions. An expansion of the $\boldsymbol{\xi}$ -dependence into spherical harmonic functions up to degree N can then be seen as a spectral method. Combining this spectral approach with a space discretization by finite elements, the set of possible solutions becomes a finite dimensional vector space and, via the weak formulation of the RTE, a Galerkin method arises.

To estimate the numerical effort of the Galerkin method, we solve the RTE on a three dimensional unit cube G with sources $f = 1$, $g = 0$, absorption rate $\sigma = 4$, and a constant reflection coefficient function $\hat{\rho} = 0.7$. The finite element discretization is based on multi-linear elements on a cubic mesh with \hat{M} degrees of freedom. The order N of the spherical harmonic expansion ranges in $\{1, \dots, 5\}$ which corresponds to $\hat{N} \in \{4, 9, 16, 25, 36\}$ degrees of freedom. We remark that in a case of high resolution $N = 5$ and $\hat{N}\hat{M} \approx 20,000$, the stiffness matrix has *about seven million non-zero elements*. Solving this large linear system is, of course, time and memory consuming and cannot be afforded in our problem where RTE solutions are required in each cycle of a heat equation solver.

3.4 The new hybrid method

Our task is to solve the radiative transfer equation repeatedly on the same geometry with changing sources. If the (integrated) absorption coefficients (see section 2) σ_k , $k = 1, \dots, M$, are of very different orders of magnitude, we will have to consider $\sigma_k \rightarrow \infty$ (“high absorption regime”) and $\sigma_k \rightarrow 0$ (“low absorption regime”).

This motivates to use two methods – one being designed for the case of high absorption rates, the other one for low absorption rates. By construction, the methods are expected to perform well in cases where σ_k is either very large or very small. For intermediate values, it is not clear which method should be preferred.

Remark 1 *In simulations one typically finds a “critical value” σ_{crit} . Whenever σ exceeds σ_{crit} , the high absorption approximation performs better than the low absorption approximation, and vice versa for σ smaller than σ_{crit} . The value of σ_{crit} , however, depends on the initial- and boundary data, on the given geometry and on the radiation sources which may vary in time.*

Therefore, it is advisable to switch between the methods with a dynamic criterion.

The decision is made by means of the residual based error formula as proposed in [9],

$$\epsilon_k(\tilde{I}_k) = \epsilon_{k,1}(\tilde{I}_k) + \epsilon_{k,2}(\tilde{I}_k), \quad k = 1, \dots, M, \quad (3.2)$$

where \tilde{I}_k is an approximate solution of (2.11), (2.12) in frequency band k , and $\epsilon_{k,1}(\tilde{I}_k)$ is the volume integrated residuum of (2.11)

$$\epsilon_{k,1}(\tilde{I}_k) := \int_{S^2 \times G} \left| \tilde{I}_k + \frac{1}{\sigma_k} \boldsymbol{\xi} \cdot \nabla \tilde{I}_k - \beta_k(T) \right|^2 d(\omega(\boldsymbol{\xi}), \mathbf{x})$$

and $\epsilon_{k,2}(\tilde{I}_k)$ is a weighted surface integral over the residuum of (2.12)

$$\epsilon_{k,2}(\tilde{I}_k) := \int_{S^2 \times \partial G} \frac{1}{\sigma_k} \frac{|\boldsymbol{\xi} \cdot \mathbf{n}(\boldsymbol{\zeta})|}{1 - \hat{\rho}^2} \left| \tilde{I}_k - \hat{\rho} \tilde{I}_k'' - (1 - \hat{\rho}) \beta_k(T_F) \right|^2 d(\omega(\boldsymbol{\xi}), \mathbf{s}(\boldsymbol{\zeta}))$$

where $\hat{\rho}$ is evaluated at $|\boldsymbol{\xi} \cdot \mathbf{n}(\boldsymbol{\zeta})|$.

Remark 2 *The proposed residuum based error formula is canonical for the following reason. Assume $k \in \{1, \dots, M\}$ and assume \tilde{I}_k is an approximate solution of (2.11), (2.12) in the sense that that \tilde{I}_k satisfies the boundary conditions (2.12) and \tilde{I}_k is sufficiently regular such that \tilde{I}_k is in the domain of the (weakly reformulated) differential operator of (2.11). Then it can be shown (see [4] for a proof) that $\epsilon_k(\tilde{I}_k) = \|I_k - \tilde{I}_k\|^2$, where I_k is the unique solution of (2.11), (2.12) and $\|\cdot\|$ is the norm canonically associated with (2.11), (2.12). Thus, for each $k \in \{1, \dots, M\}$, the residuum based error formula (3.2) is an excellent measure for the accuracy of the approximation \tilde{I}_k .*

The combined method with a switch based on the residual based error formula (3.2) is called *hybrid method* in the following.

Note that it is also possible to combine the residua $\epsilon_{k,1}$ and $\epsilon_{k,2}$ in different proportions. In this way, one obtains error formulas which focus, for example, more on boundary terms than on volume terms. However, we will not investigate this aspect and stick to the canonical form (3.2).

In the high absorption regime a two-scale analysis of (2.11), (2.12) has been performed in [9]. As a result, for large values of σ_k , an approximation of the radiative intensity corresponding to a given temperature profile $T = T(t, \mathbf{x})$ is given by

$$I_k^{high}(t, \boldsymbol{\xi}, \mathbf{x}) = \beta_k(T_F) + (\beta_k(T(t, \mathbf{x})) - \beta_k(T_F)) I_{k,0}(\boldsymbol{\xi}, \mathbf{x}) \\ + (\partial_T \beta_k)(T(t, \mathbf{x})) \sum_{j=1}^3 (\partial_{x_j} T)(t, \mathbf{x}) (I_{k,j}(\boldsymbol{\xi}, \mathbf{x}) - x_j I_{k,0}(\boldsymbol{\xi}, \mathbf{x})), \quad (3.3)$$

where $I_{k,j}$, $j = 0, \dots, 3$, are time and data independent solutions of the reference problems

$$\frac{1}{\sigma_k} \boldsymbol{\xi} \cdot \nabla_{\mathbf{x}} I_{k,j} + I_{k,j} = \begin{cases} 1 & \text{if } j = 0 \\ x_j & \text{if } j \in \{1, 2, 3\} \end{cases}, \quad \text{on } G \times S^2, \quad (3.4)$$

subject to the boundary conditions

$$I_{k,j}(\boldsymbol{\xi}, \boldsymbol{\zeta}) - \hat{\rho}(|\boldsymbol{\xi} \cdot \mathbf{n}(\boldsymbol{\zeta})|) I_{k,j}(\boldsymbol{\xi}'', \boldsymbol{\zeta}) = 0, \quad \text{for } (\boldsymbol{\zeta}, \boldsymbol{\xi}) \in S^-. \quad (3.5)$$

Based on I_k^{high} , we calculate the radiative flux

$$\mathbf{F}_k^{high}(t, \mathbf{x}) = \int_{S^2} \boldsymbol{\xi} I_k^{high}(\boldsymbol{\xi}, \mathbf{x}) d\omega(\boldsymbol{\xi})$$

whose divergence is needed on the right hand side of (2.10). Note that \mathbf{F}_k^{high} can be expressed in terms of the fixed moments of the reference solutions $I_{k,j}$.

In the low absorption regime, asymptotic expansions are of little help for the construction of fast methods. In lowest order, the intensity is constant $I^{(0)} = n_m^2 \beta(T_F)$ (see [9]) and equations for higher order corrections are of the same type as the RTE which rules out the derivation of explicit expressions.

Instead of an asymptotic expansion, we use a heuristic argument: formula (3.1) suggests that, for small σ , the intensity at a point $\mathbf{x} \in G$ is essentially given by some averaged

source term. In particular, small fluctuations in the source seem to be less important in the case $\sigma \rightarrow 0$ and it might be reasonable to approximate the source with a low order polynomial. Following [9], we obtain for an approximation with affine polynomials (the method can easily be extended to higher order approximations),

$$I_k^{proj}(t, \boldsymbol{\xi}, \mathbf{x}) = (1 - I_{k,0}(\boldsymbol{\xi}, \mathbf{x}))\beta_k(T_F) + \sum_{j=0}^3 b_{k,j}(t)I_{k,j}(\boldsymbol{\xi}, \mathbf{x}),$$

where the coefficients $b_{k,j}(t)$ are chosen by *projecting* $\beta_k(T)$ onto the space of affine polynomials, i.e. by minimizing the \mathbb{L}^2 distance

$$\int_G |b_{k,0}(t) + \sum_{j=1}^3 b_{k,j}(t)x_j - \beta_k(T(t, \mathbf{x}))|^2 d\mathbf{x} \quad (3.6)$$

which leads to a linear 4×4 system. Since I_k^{proj} is an exact solution of the RTE with a modified source, the divergence of the corresponding radiative flux \mathbf{F}_k^{proj} follows from the $\boldsymbol{\xi}$ -integrated RTE,

$$\begin{aligned} \operatorname{div} \mathbf{F}_k^{proj}(t, \mathbf{x}) &= \operatorname{div} \int_{S^2} \boldsymbol{\xi} I_k^{proj}(\boldsymbol{\xi}, \mathbf{x}) d\omega(\boldsymbol{\xi}) \\ &= 4\pi\sigma \left(b_{k,0}(t) + \sum_{j=1}^3 b_{k,j}(t)x_j \right) + \sigma \int_{S^2} I_k^{proj}(\boldsymbol{\xi}, \mathbf{x}) d\omega(\boldsymbol{\xi}). \end{aligned} \quad (3.7)$$

Here, only the $\boldsymbol{\xi}$ integral over I_k^{proj} is required. These integrals can be written in terms of the coefficients $b_{k,j}$ and the $\boldsymbol{\xi}$ integrals over the reference solutions $I_{k,j}$.

Practically, the solutions $I_{k,j}$ are obtained with an accurate method like ray tracing based on many directions (≥ 100) and many reflections (≥ 10). This large effort has to be taken only once in a pre-processing step. Moreover, we only store the moments of the pre-processed solutions $I_{k,j}$ which reduces the memory consumption and speeds up the evaluation of the fluxes in each cycle of the heat equation solver.

Let us now turn to the question how to combine the two methods into a single hybrid method. We use the normed residuum of (3.2) for the k th frequency band. If I_k^{proj} and I_k^{high} are the approximations obtained with the two methods in frequency band k , we compare $\epsilon_k(I_k^{proj})$ and $\epsilon_k(I_k^{high})$ (evaluated by approximate quadrature rules) to select the more accurate solution for which the flux divergence for frequency band k is calculated.

For the projection method one can show [9]

$$\epsilon_k(I_k^{proj}) = 4\pi \int_G |b_{k,0}(t) + \sum_{j=1}^3 b_{k,j}(t)x_j - \beta_k(T(t, \mathbf{x}))|^2 d\mathbf{x} \quad (3.8)$$

which is, up to a constant, the projection error (3.6). In particular, the explicit knowledge of $I_k^{proj}(\mathbf{x}, \boldsymbol{\xi})$ is neither required for the normed residuum nor for the evaluation of the flux divergence. Thus, one would like to avoid storing the reference solutions corresponding to polynomial sources. As a consequence, one should try to approximate $\epsilon_k(I_k^{high})$ by zero and first order $\boldsymbol{\xi}$ moments of $I_{k,j}$ or, using linearity, by

$$E_k^{high}(\mathbf{x}) = \int_{S^2} I_k^{high}(\mathbf{x}, \boldsymbol{\xi}) d\boldsymbol{\xi}, \quad \mathbf{F}_k^{high}(\mathbf{x}) = \int_{S^2} \boldsymbol{\xi} I_k^{high}(\mathbf{x}, \boldsymbol{\xi}) d\boldsymbol{\xi}.$$

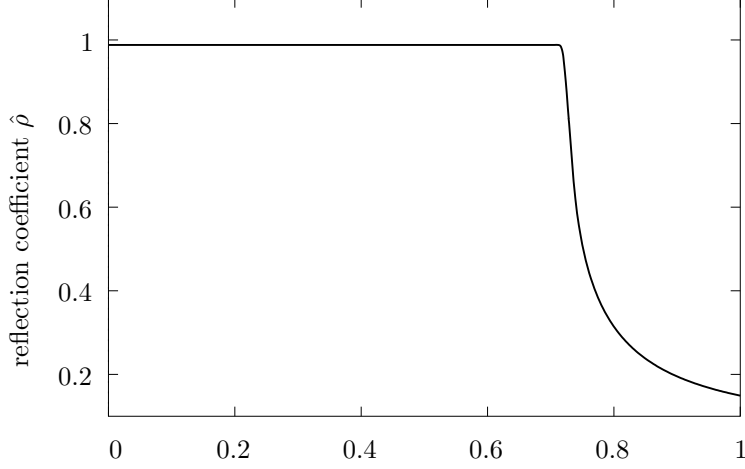


FIGURE 1. FRESNEL-type reflection coefficient function

Following the argument in [9], such an approximation is indeed available,

$$\epsilon_k(I_k^{high}) \approx \epsilon_k^{high} = \epsilon_{k,1}^{high} + \epsilon_{k,2}^{high},$$

where $\epsilon_{k,1}^{high}$ is a contribution from volume integrals over the $\boldsymbol{\xi}$ moments

$$\begin{aligned} \epsilon_{k,1}^{high} = & \int_G \frac{1}{4\pi} \left(E_k^{high} - 4\pi\beta_k(T) \right)^2 + \frac{3}{4\pi} \left| \mathbf{F}_k^{high} \right|^2 + \frac{1}{4\pi\sigma_k^2} \left(\operatorname{div} \mathbf{F}_k^{high} \right)^2 \\ & + \frac{1}{12\pi\sigma_k^2} \left| \nabla E_k^{high} \right|^2 - \frac{2}{\sigma_k} \operatorname{div} \mathbf{F}_k^{high} (\beta_k(T) - \beta_k(T_F)) \, d\mathbf{x} \end{aligned}$$

and $\epsilon_{k,2}^{high}$ a contribution from surface integrals

$$\begin{aligned} \epsilon_{k,2}^{high} = & \int_{\partial G} \frac{1}{\sigma_k} \left(\int_{S^2} \frac{1}{|\boldsymbol{\xi} \cdot \mathbf{n}|} \frac{1+\rho(\boldsymbol{\xi} \cdot \mathbf{n})}{1-\rho(\boldsymbol{\xi} \cdot \mathbf{n})} \, d\boldsymbol{\xi} \right)^{-1} \left(E_k^{high} - 4\pi n_m^2 B(T_F) \right)^2 \\ & + \frac{1}{\sigma_k} \left(\int_{S^2} |\boldsymbol{\xi} \cdot \mathbf{n}| \frac{1-\rho(\boldsymbol{\xi} \cdot \mathbf{n})}{1+\rho(\boldsymbol{\xi} \cdot \mathbf{n})} \, d\boldsymbol{\xi} \right)^{-1} \left(\mathbf{n} \cdot \mathbf{F}_k^{high} \right)^2 \, d\zeta. \end{aligned}$$

In order to obtain an impression of the quality of the projection and high absorption method as well as the approximation ϵ_k^{high} of the normed residuum, we consider an example with slab geometry for a medium of optical density $n_m = 1.46$. As sources, we consider here the artificial cases $B(T(\mathbf{x})) = x_1^2$, $x_1 \in [-1, 1]$, $x_2, x_3 \in \mathbb{R}$ and $B(T_F) = 0$. The reflection function is of FRESNEL-type (see fig. 1) with $\hat{\rho}(\mu) = \bar{\rho}$ being almost equal to one for $\mu \leq 1 - 1/n_m^2$. We remark that the classical FRESNEL law includes total reflection (i.e. $\hat{\rho}(\mu) = 1$ for $\mu \leq 1 - 1/n_m^2$). We exclude the case of total reflection in the following by assuming $\bar{\rho} < 1$. However, numerical experiments indicate that the error formula works well also in the limit case where total reflection appears on parts of the boundary, provided that the set $\{(\boldsymbol{\xi}, \mathbf{x}) : \hat{\rho}(|\boldsymbol{\xi} \cdot \mathbf{n}(\mathbf{x})|) = 1\}$ is excluded from the integration domain in $\epsilon_{k,2}$.

The errors in figure 2 are normalized by the error of the zero-intensity function. The convergence of the high absorption method for large absorption rates σ can clearly be

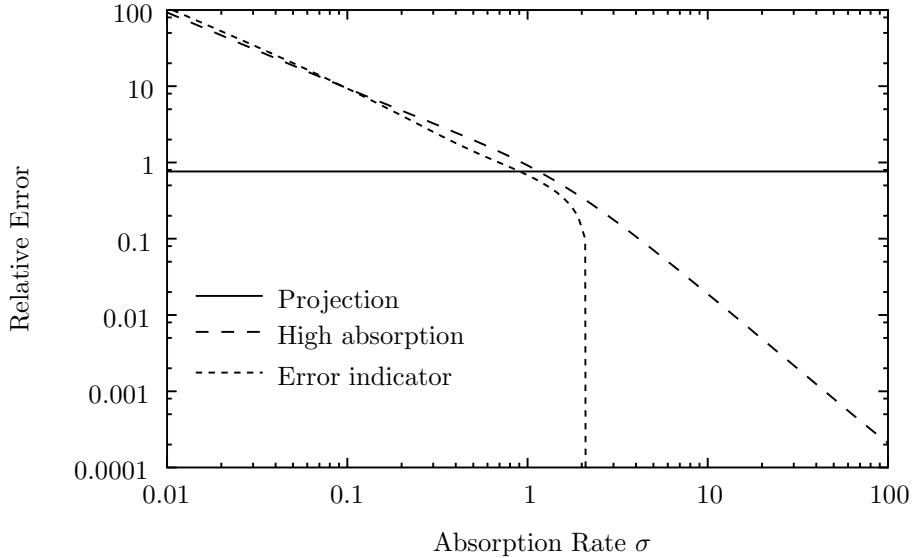


FIGURE 2. Comparison of Relative Errors

observed. On the other hand, the projection method does not converge for $\sigma \rightarrow 0$ but yields a better approximation for small σ than the other method. In view of (3.8), convergence is only expected for increasing accuracy in the \mathbb{L}^2 approximation. Note, however, that the intensity average $E_k^{proj} = \int I_k^{proj} d\omega(\boldsymbol{\xi})$ (which is the quantity we actually use in (3.7)) converges to the correct value for $\sigma \rightarrow 0$ (see [9]).

The approximative error for the high absorption method (denoted by *error indicator* in the figure) is acceptable in the region where both methods are of similar quality. It only overestimates the quality in a region where the high absorption method is anyhow better. Thus, in order to save memory and computational time, the error indicator can be used instead of the normed residuum for the high absorption method.

3.5 The cooling problem

We consider a small glass cylinder of height 5cm and radius 10cm . The cylinder has a constant initial temperature distribution of 1500°C and is placed in a background medium of constant reference temperature $T_F = 20^\circ\text{C}$. The reflection coefficient function is shown in fig. 1 and the remaining material properties have been chosen according to Table 1. The absorption rate $\sigma(\nu)$ is approximated by a piece-wise constant function (see Fig. 3) consisting of 20 frequency bands. The last frequency band ($\nu > 1.5 \cdot 10^{16}\text{Hz}$) is neglected because the sources in the RTE practically vanish for these frequencies in connection with the temperatures considered here, resulting in negligible intensity contributions. In the first band ($\nu < 4.2 \cdot 10^{13}\text{Hz}$), we assume $\sigma = \infty$. This case can be treated easily with the high absorption method which has been derived for the limiting case $\sigma \rightarrow \infty$. The required reference solutions for this frequency band simplify to the zero-order approximations in the limit $\sigma \rightarrow \infty$. For the remaining frequency bands, we solve equation (2.11) with the

Specific Heat Capacity	$c_v = 1.2 \cdot 10^3 \frac{J}{kg K}$
Mass Density	$\rho_m = 2.5 \cdot 10^3 \frac{kg}{m^3}$
Thermal Conductivity	$\kappa = 1.7 \frac{W}{K m}$
Refraction Index	$n_g = 1.46$

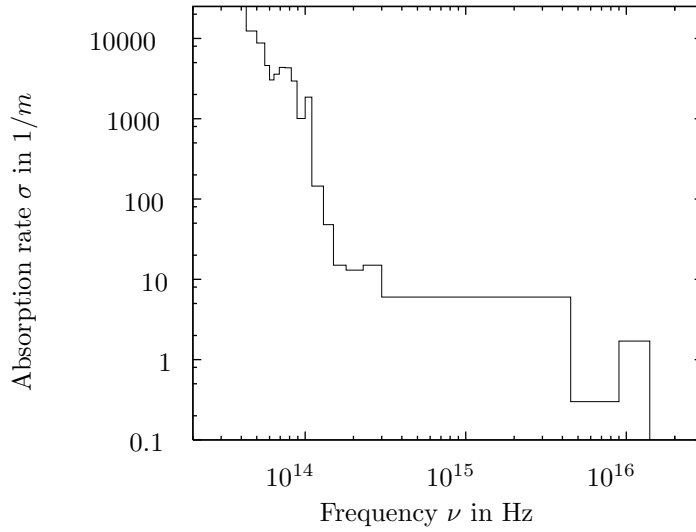
Table 1. *Properties of the glass*

FIGURE 3. Absorption rate as function of the frequency

corresponding values for σ_k where the normed residuum is used to decide which method is applied.

We remark that the initial temperature difference is artificial as it would lead to a breaking of the glass. Nevertheless, we choose the example to show that our method is able to properly resolve strong boundary layers in the temperature profile (see figure 4 for the temperature distribution obtained with the hybrid method after 10s). The heat equation has been approximated with a finite element discretization using the cylinder symmetry of the problem (5100 degrees of freedom – 100 in radial and 51 in vertical direction). The solution of the hybrid method is based on particular solutions obtained with the ray tracing method where in each node, 120 rays have been traced backwards, taking into account 10 reflections at the boundaries. To get a quantitative comparison of different methods, we also plot the temperature distribution on paths along the height, the radius and the diagonal of the cylinder (see fig. 5). The temperature obtained with the hybrid method in comparison to a ray tracing solution (which is calculated with only 10 directions and two reflections at the boundaries to get a manageable speed) and the first order ROSSELAND approximation is given in the figures 6, 7, and 8. Note that a direct comparison of the radiative intensities based on the normed residuum is complicated by

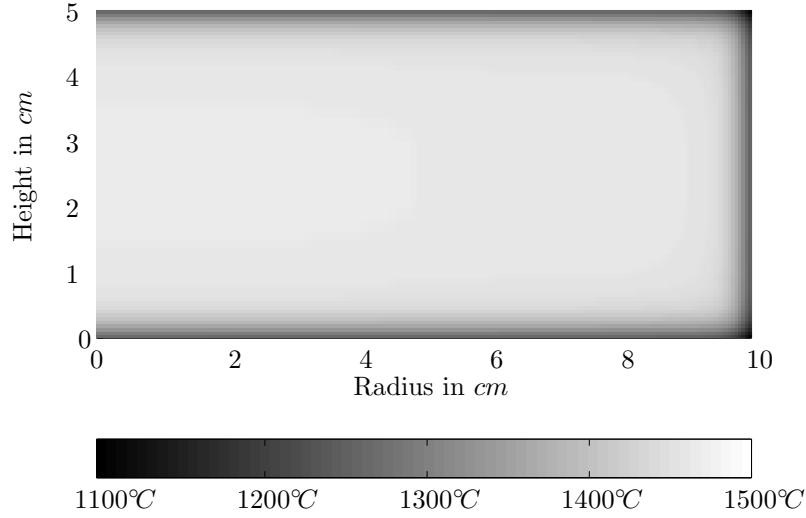


FIGURE 4. Temperature distribution in a section of the glass cylinder

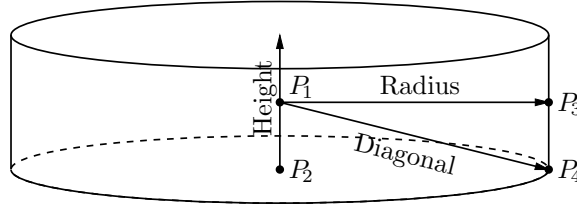


FIGURE 5. Selected paths and points in the cylinder

the fact that the ray-tracing algorithm yields intensities only at discrete points, so that the value of the residuum norm depends on the chosen interpolation.

The profiles show that the hybrid method approximates well the overall cooling of the bulk. The difference to the ray tracing solution in the center of the cylinder (P_1) is only 2.9°C (that is less than 0.2%). The rapid cooling at the boundary is also captured well by the hybrid method with a difference to the ray tracing method of 3.2°C at (P_2) and of 4.5°C at the point (P_3). Even the temperature in the edge of the cylinder (P_4) is approximated well with a difference to the ray tracing solution of 10.4°C . The first order ROSSELAND approximation which is commonly applied in industrial applications fails completely for the chosen initial conditions.

We close with a remark concerning the selection of the methods. Initially, the temperature distribution is constant inside the glass and both methods yield the same solution. In this case, the high absorption method is used in all frequency bands. Already in the second time step, the temperature distribution is no longer uniform and the selection mechanism based on the normed residuum starts to distribute frequency bands also on the projection method. Eventually, the frequency bands 0 to 11 are treated with the high absorption method. The remaining frequencies are taken care of by the projection method. From time to time, the intermediate band number 11 switches from high ab-

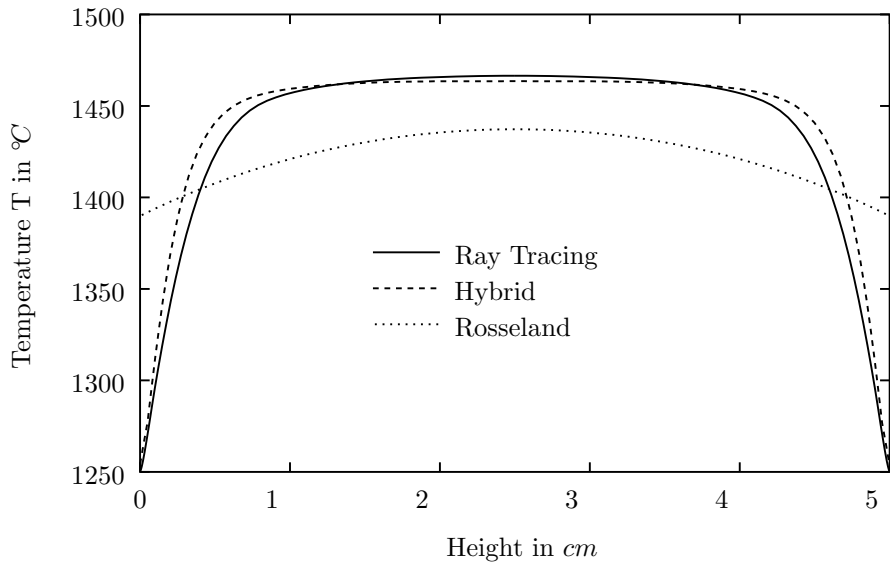


FIGURE 6. Temperature in vertical direction

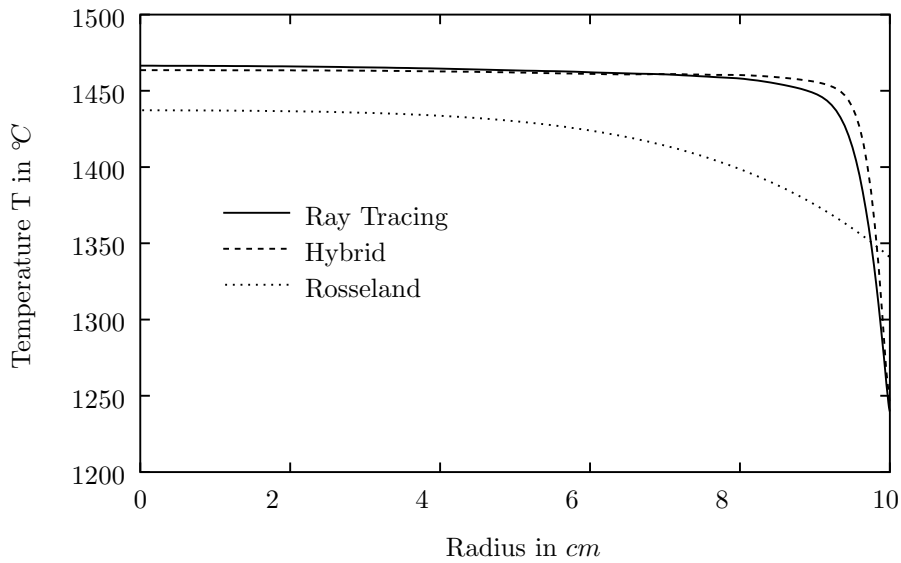


FIGURE 7. Temperature along the radius

sorption method to projection method. Compared to the (admittedly crude) ray tracing algorithm, the speed up factor is around 50. The ROSSELAND approximation is again faster by a factor 1.5, but its quality is not acceptable.

4 Conclusion

The simulation of cooling processes in glass production requires a fast solver of the radiative transfer equation. We construct an efficient hybrid method using two methods which

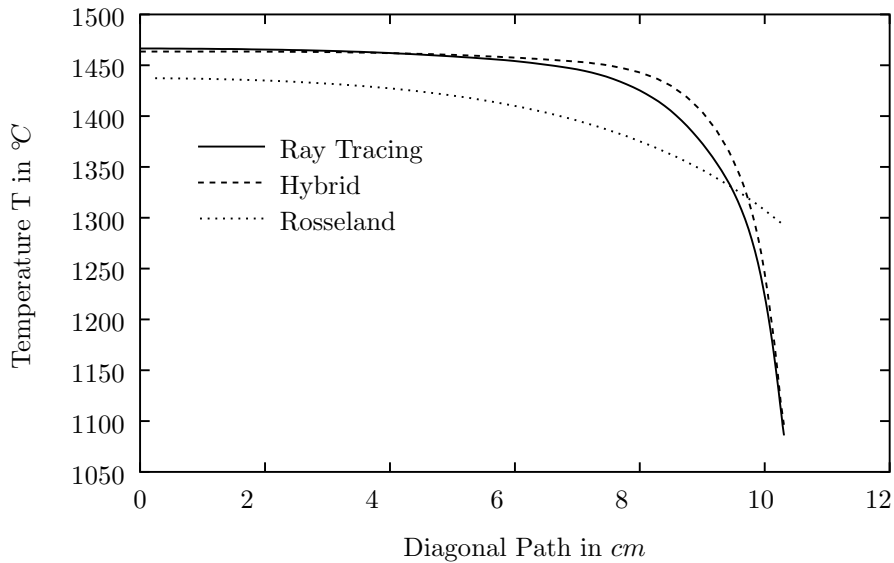


FIGURE 8. Temperature along the diagonal

are designed for high and low absorption rates respectively. The core of the scheme is a residual based error formula for the radiative transfer equation which allows a dynamical switching between the two methods in each frequency band.

In practical applications, long cooling periods (several minutes) have to be simulated. Here, the hybrid scheme requires additional tuning. For example, the approximation of the normed residuum can be simplified further and its evaluation can be restricted to the critical frequency bands (leading to speed up factors from 100 to 200 compared to ray tracing). Despite these simplifications, the method remains more accurate than the ROSSELAND approximation which is widely used for the applications considered here. Since the application of standard methods like ray tracing or P_N approximations is completely out of scope for long-time simulations, the hybrid method is a substantial progress.

Acknowledgement

The numerical parts of this work have been carried out in the framework of F. Zingsheim's Ph.D. project at the *Institut für Techno- und Wirtschaftsmathematik (ITWM)* at Kaiserslautern, Germany. The financial support of the ITWM and the *Stiftung-Rheinland Pfalz für Innovation* is gratefully acknowledged.

References

- [1] M. K. Choudhary and N. T. Huff. Mathematical modeling in the glass industry: An overview of status and needs. *Glastechnische Berichte (Glass science and technology)*, 70(12):363–370, 1997.
- [2] R. Dautray and J.-L. Lions. *Evolution Problems II*, volume 6 of *Mathematical Analysis and Numerical Methods for Science and Technology*. Springer-Verlag, Berlin Heidelberg, 1993.

- [3] F. C. Lockwood and N. G. Shah. A new radiation solution method for incorporation in general combustion prediction procedures. In *Eighteenth Symposium (International) on Combustion*, pages 1405–1414. The Combustion Institute, 1981.
- [4] M. Junk, A. Unterreiter and F. Zingsheim. A Residual Based Error Formula for a Class of Transport Equations. *submitted*, 2001.
- [5] M. F. Modest. *Radiative heat transfer*. McGraw-Hill series in mechanical engineering. McGraw-Hill, New York, 1993.
- [6] R. Siegel and J. R. Howell. *Thermal radiation heat transfer*. Hemisphere Publishing Corporation, Washington, 1992.
- [7] R. Viskanta and E. E. Anderson. Heat Transfer in Semitransparent Solids. *Advances in heat transfer*, 11:317–441, 1975.
- [8] F. E. Woolley. R&D Needs in Glass Melting Physics and Chemistry. In H. A. Schaeffer and R. G. C. Beerkens, editors, *Melting Processes in Glass Furnaces*, pages 1–6, 1998. Proceedings of the HVG/NCNG Colloquium.
- [9] F. Zingsheim. *Numerical Solution Methods for Radiative Transfer in Semitransparent Media*. PhD thesis, University of Kaiserslautern, 1999.